

# Response of LNCaP Spheroids after Treatment with an $\alpha$ -Particle Emitter ( $^{213}\text{Bi}$ )-labeled Anti-Prostate-specific Membrane Antigen Antibody (J591)<sup>1</sup>

Åse M. Ballangrud, Wei-Hong Yang, David E. Charlton, Michael R. McDevitt, Klaus A. Hamacher, Katherine S. Panageas, Dangshe Ma, Neil H. Bander,<sup>2</sup> David A. Scheinberg, and George Sgouros<sup>3</sup>

Departments of Medical Physics [Å. M. B., W-H. Y., K. A. H., G. S.], Medicine [M. R. M., D. M., D. A. S.], and Epidemiology and Biostatistics [K. S. P.], Memorial Sloan-Kettering Cancer Center, New York, New York 10021; Weill Medical College of Cornell University, New York, New York 10021 [N. H. B.]; and Physics Department, Concordia University, Montreal, Quebec, Canada [D. E. C.]

## ABSTRACT

A theoretical drawback to  $\alpha$ -particle therapy with  $^{213}\text{Bi}$  is the short range of the particle track coupled with the short half-life of the radionuclide, thereby potentially limiting effective cytotoxicity to rapidly accessible, disseminated individual tumor cells (e.g., as in leukemia). In this work, a prostate carcinoma spheroid model was used to evaluate the feasibility of targeting micrometastatic clusters of tumor cells using  $^{213}\text{Bi}$ -labeled anti-prostate-specific membrane antigen (PSMA) antibody, J591. In prostate cancer, vascular dissemination of tumor cells or tumor cell clusters to the marrow constitutes an important step in the progression of this disease to widespread skeletal involvement, an incurable state. Such prevascularized clusters are ideal targets for radiolabeled antibodies because the barriers to antibody penetration that are associated with the capillary basal lamina have not yet formed.  $\beta$ - and  $\gamma$ -emitting radionuclides such as  $^{131}\text{I}$ , which are widely used in radioimmunotherapy, are not expected to be effective when targeting single cells or small cell clusters. This is because the range of the emissions is one to two orders of magnitude greater than the target size, and the energy deposited per traversal is insufficient to produce any significant radiobiological effect. Spheroids of the prostate cancer cell line, LNCaP-LN3, were used as a model of prevascularized micrometastases; their response to an anti-PSMA antibody, J591, radiolabeled with the  $\alpha$ -particle emitter  $^{213}\text{Bi}$  ( $T_{1/2}$ , 45.6 min.) has been measured. The time course of spheroid volume reductions was found to be sensitive to the initial spheroid volume. J591 labeled with 0.9 MBq/ml  $^{213}\text{Bi}$  resulted in a 3-log reduction in spheroid volume on day 33, relative to control, for spheroids with an initial diameter of 130  $\mu\text{m}$ ; 1.8 MBq/ml were required to achieve a similar response for spheroids with an initial diameter of 180  $\mu\text{m}$ . Equivalent spheroid responses were observed after 12 Gy of acute external beam photon irradiation. Monte Carlo-based microdosimetric analyses of the  $^{213}\text{Bi}$  decay distribution in individual spheroids of 130- $\mu\text{m}$  diameter yielded an average  $\alpha$ -particle dose of 3.7 Gy to the spheroids, resulting in a relative biological effectiveness factor of 3.2 over photon irradiation. The activity concentrations used in the experiments were clinically relevant, and this work supports the possibility of using  $^{213}\text{Bi}$ -labeled antibodies not only for disseminated single tumor cells, as found in patients with leukemia, but also for micrometastatic tumor deposits up to 180  $\mu\text{m}$  in diameter (1200 cells).

## INTRODUCTION

Radiolabeled antibody therapy has already demonstrated efficacy in the treatment of non-Hodgkin's lymphoma (1–3). Results have been largely disappointing, however, in the targeting of bulky disease. To target bulky disease, i.v. administered antibody must extravasate, diffuse across an interstitial fluid space, and then distribute throughout

antigen-positive cells. Each of these steps is associated with a barrier to delivery (4–9). By targeting hematologically distributed, single tumor cells or tumor cell clusters, the barriers to antibody delivery are diminished.

$\beta$ -Particle-emitting radionuclides such as  $^{131}\text{I}$  and  $^{90}\text{Y}$  have been used in most applications of radioimmunotherapy. These radionuclides are suboptimal for sterilizing single tumor cells or small tumor cell clusters because the concentration of radioactivity required to provide the thousands to tens of thousands of  $\beta$ -particle traversals through the cell nucleus needed to achieve cytotoxicity would also yield prohibitive normal organ toxicity.  $\alpha$ -Particles are much more cytotoxic than  $\beta$ -particles and would, therefore, be ideal candidates in targeting individual tumor cells or small clusters. The effectiveness of  $\alpha$ -particles arises because the amount of energy deposited per unit distance traveled (linear energy transfer) can be several orders of magnitude greater than that of  $\beta$ -particles. Cell survival studies have shown that  $\alpha$ -particle-induced killing is independent of oxygenation state or cell cycle during irradiation (10, 11).

Spheroids have been used by a number of investigators as models of tumor cell micrometastases (12–17). These multicellular clusters provide the experimental flexibility of monolayer cultures while preserving the three-dimensional structure that is important for the cell-to-cell interaction that exists *in vivo*. The spheroid model is particularly important in establishing a relationship between antibody binding kinetics, antigen density, internalization, and external antibody concentration, as well as to assess kill probability under different antibody concentrations and specific activities. It is an ideal model to optimize treatment parameters. Such optimization is essential in the treatment of micrometastases because objective measures of response will not be generally available *in vivo*.

Previous spheroid studies with large (800- $\mu\text{m}$ -diameter) spheroids using antibodies labeled with the  $\alpha$ -particle emitter,  $^{212}\text{Bi}$ , concluded that this  $\alpha$ -particle emitter would be ineffective because the short, 50–90- $\mu\text{m}$  range of the  $\alpha$ -particles, coupled with the short, 1-h half-life, restricted tumor cell targeting (18). The requirement of adequate oxygen and nutrient supply, however, limits prevascularized micrometastases to maximum diameters of 150–200  $\mu\text{m}$ . The emission properties of  $^{213}\text{Bi}$  (Fig. 1) used in the experiments reported here are similar to those of  $^{212}\text{Bi}$ , with the exception that  $^{213}\text{Bi}$  does not emit the highly energetic and penetrating photon emissions found in  $^{212}\text{Bi}$ . Recently, Kennel *et al.* (19) compared surviving fraction of cells in monolayers and in spheroids irradiated by surface-bound  $^{213}\text{Bi}$ . These studies were carried out using spheroids derived from the murine EMT6 cell line and the 13A antibody against murine CD44. Tumor cells in spheroids were efficiently killed for spheroids up to 20–30 cells in diameter. Animal studies have also been performed and show that  $\alpha$ -particle emitters yield superior tumor control relative to  $\beta$  or Auger electron emitters (10, 20–23). Human use of  $\alpha$ -particle emitters has also been reported (24–26). The first implementation was with  $^{213}\text{Bi}$  conjugated to the anti-CD33 antibody, HuM195, targeting myeloid leukemia. This trial demonstrated feasibility and anticancer activity with minimal toxicity (24). The anti-tenascin antibody, 81C6,

Received 8/8/00; accepted 1/3/01.

The costs of publication of this article were defrayed in part by the payment of page charges. This article must therefore be hereby marked *advertisement* in accordance with 18 U.S.C. Section 1734 solely to indicate this fact.

<sup>1</sup> Supported, in part, by NIH Grants PO1 CA-33049, R01 CA-55349, and R01 CA-72683 and also by the CapCure Foundation. D. A. S. is the recipient of the Doris Duke Distinguished Clinical Scientist Award.

<sup>2</sup> N. H. B. is a consultant to BZL Biologics, Inc. His association with BZL is managed in accordance with the conflict of interest policies of Cornell University.

<sup>3</sup> To whom requests for reprints should be addressed, at Department of Medical Physics, Memorial Sloan-Kettering Cancer Center, 1275 York Avenue, New York, NY 10021. E-mail: sgouros@mskcc.org.

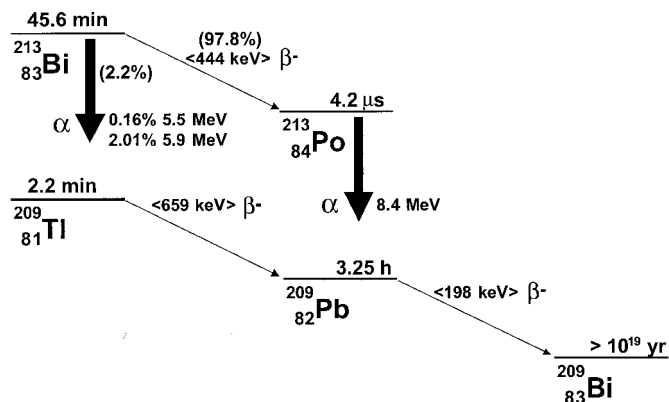


Fig. 1. <sup>213</sup>Bi decay scheme.

labeled with the α-particle emitter, <sup>211</sup>At, has been injected into surgically created cavities in patients with malignant gliomas. This trial has demonstrated substantially better tumor control relative to <sup>131</sup>I-labeled 81C6 antibody (27).

Fifty to 60% of prostate cancer patients either present with or develop metastases in the course of their disease. Of those that metastasize, bone involvement occurs in >80% of cases (28). The unique propensity of prostatic epithelial cells to seed in the bone marrow and, in advanced disease, to disseminate as small (rapidly accessible) clusters, eventually invading the bone matrix to become skeletal metastases (29), forms a compelling rationale for investigating <sup>213</sup>Bi radioimmunotherapy against prostate cancer. In this study, spheroids of the prostate carcinoma cell line LNCaP-LN3 are used to investigate the potential efficacy and to optimize the use of <sup>213</sup>Bi-labeled anti-PSMA<sup>4</sup> antibody in targeting disseminated prostate cancer micrometastases.

**MATERIALS AND METHODS**

**Cells.** LNCaP-LN3 cells were provided by Drs. Curtis Pettaway and Isaiah Fidler of the M. D. Anderson Cancer Center. LNCaP cells of the LN3 subline exhibit a highly metastatic potential and produce all three prostatic biomarkers: prostatic acid phosphatase, prostate-specific antigen, and PSMA (30–32). The cells are hormonally responsive to testosterone, express high affinity to androgen receptors, and are tumorigenic in nude mice. Monolayer cultures were incubated in RPMI 1640 (Life Technologies, Inc., Grand Island, NY), supplemented with 10% fetal bovine serum (Gemini Bio-Products, Inc., Woodland, CA), 100 units/ml penicillin, and 100 μg/ml streptomycin. The cell cultures were kept at 37°C in a humidified 5% CO<sub>2</sub> and 95% air incubator.

**Spheroids.** Spheroids were initiated using the liquid overlay technique of Yuhas *et al.* (33). Details regarding LNCaP spheroid formation and characterization are described in Ballangrud *et al.* (17). Approximately 10<sup>6</sup> LNCaP-LN3 cells, obtained by trypsinization from growing monolayer cultures, were seeded into 100-mm dishes coated with a thin layer of 1% agar (Bacto Agar; Difco, Detroit, MI) with 15 ml of RPMI 1640, supplemented with 10% fetal bovine serum, 100 units/ml penicillin, and 100 μg/ml streptomycin. After 3–4 days, spheroids of approximate diameters 130 ± 20 μm and 180 ± 20 μm were selected under an inverted phase-contrast microscope with an ocular scale using an Eppendorf pipette. The selected spheroids were transferred to 35-mm bacteriological Petri dishes in 2 ml of medium for treatment.

**Antibodies.** The anti-PSMA antibody, J591, used in these experiments targets the external domain of PSMA (34). PSMA is expressed on the surface of the original LNCaP cells at a density of ~180,000 sites/cell (35, 36). Using a modified Scatchard analysis (37), an antigen site density for the LN3 subline of 130,000 sites/cell was measured. PSMA expression has also been found in

tumor but not in normal vascular endothelium (34, 38). The anti-CD33 antibody, HuM195 (39, 40), was used as a nonspecific control.

**<sup>213</sup>Bi Labeling.** The isothiocyanatobenzyl derivative of CHXA-DTPA (41–43) was used to chelate <sup>213</sup>Bi to the two antibodies. The radionuclide was available from an <sup>225</sup>Ac/<sup>213</sup>Bi generator that was obtained from the Transuranic Research Institute (Karlsruhe, Germany) and the United States Department of Energy. Details regarding the <sup>225</sup>Ac/<sup>213</sup>Bi generator and the chelation of <sup>213</sup>Bi to antibodies have been published previously (44, 45). The specific activity was 92.5 GBq/g (2.5 Ci/g) for both <sup>213</sup>Bi-J591 and <sup>213</sup>Bi-HuM195. Purity was 86% for <sup>213</sup>Bi-J591 and 98% for <sup>213</sup>Bi-HuM195.

**Treatment Protocol.** Spheroids were incubated with 0.9 and 1.8 MBq/ml <sup>213</sup>Bi on 10 μg/ml J591 (specific antibody) or HuM195 (hot control) for 15, 30, and 60 min and 24 h. Twenty-four spheroids were used in each experiment; after each incubation period, the spheroids were washed three times by suspension in fresh medium and placed in separate wells of a 24-well plate. Spheroids exposed to 10 μg/ml unlabeled J591 (cold control) and unexposed spheroids (control) were followed in the same manner. The medium in each well was replaced, and individual spheroid volume measurements were performed twice per week. An inverted phase microscope fitted with an ocular micrometer was used to determine the major and minor diameter *d*<sub>max</sub> and *d*<sub>min</sub>, respectively, of each spheroid. Spheroid volume was calculated as  $V = \pi \cdot d_{max} \cdot d_{min}^2 / 6$ . Volume monitoring was stopped once a spheroid had broken up or fragmented to individual cells or two to three cell clusters.

**External Beam Irradiation.** Spheroids were exposed to acute doses of 9 and 12 Gy external beam photon irradiation using a Cesium irradiator at a dose rate of 0.8 Gy/min (Cs-137 Model 68; JL Shepherd and Associates, Glendale, CA.). Volume measurements of 24 spheroids at each dose level were performed as described above.

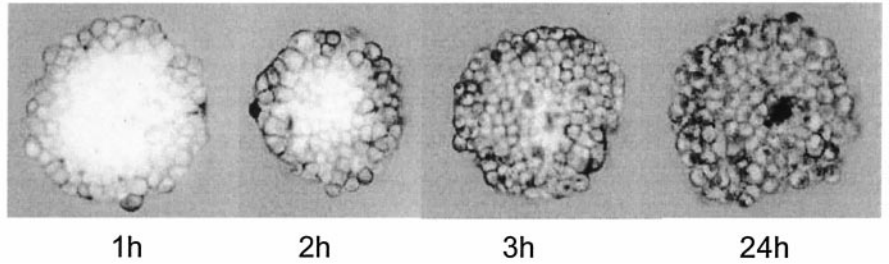
**Antibody Penetration.** Spheroids of diameter 200 μm were incubated with 10 μg/ml FITC (F7250; Sigma Chemical Co., St. Louis, MO.)-conjugated J591 for 1, 2, 3, and 24 h and imaged by confocal microscope while still in the incubation medium. A 3-μm-thick optical section was acquired at the center of each spheroid. Five spheroids were imaged for each time point. Antibody concentration as a function of radial distance was obtained using MIAU, a software package developed in-house (46). Briefly, a circular erosion element was used to follow the exterior contour of each spheroid and delineate rings of 5-μm thickness. The average pixel intensity in each ring was converted to antibody concentration by calibration with the known external concentration of antibody. The antibody concentration as a function of distance from the rim of the spheroid was corrected for light attenuation. Confocal microscope images of the equator plane of spheroids derived from cells transfected with green fluorescent protein were used to determine an attenuation correction dependent on the diameter of the spheroid. The spatial distribution of antibody concentration after different incubation durations was then used to calculate the radial distribution of α emissions for dosimetry.

**Dosimetry.** The specific activity of the antibody was used to convert the radial distribution of antibody concentration to a radioactivity concentration that, in turn, was converted to a spatial distribution of <sup>213</sup>Bi decays by integrating the radioactivity concentration profiles over time. Absorbed dose in the spheroids was calculated by the Monte Carlo method described by Charlton (47). Monte Carlo simulations were used to provide the energy and direction of the α-particles originating from the <sup>213</sup>Bi decay distribution. The chord length of α-particle traversals through the spheroid was converted to energy deposition using the stopping powers data of Ziegler (48). This approach was also used to obtain the radial distribution of absorbed dose across the spheroid, as well as the mean absorbed dose over the whole spheroid volume; the former was obtained as the mean absorbed dose in 5-μm-thick shells.

**Statistical Analysis.** Differences in tumor volumes over time were analyzed using generalized estimating equation methodology (49). This method assesses differences in groups over time while accounting for the correlation within each spheroid. Approximately 25 time points were recorded on 24 spheroids/treatment strategy. Each treatment strategy was compared with the control group. In addition, <sup>213</sup>Bi-J591 for 24 h was compared with the 12-Gy group, and <sup>213</sup>Bi-J591 for 60 min was compared with the 9-Gy group. The *P* values were adjusted for multiple comparisons by the Bonferroni correction.

<sup>4</sup> The abbreviation used is: PSMA, prostate-specific membrane antigen.

Fig. 2. Confocal microscopy slices through the equator of 200-μm-diameter LNCaP-LN3 spheroids after incubation with 10 μg/ml J591-FITC for 1, 2, 3, and 24 h.



**RESULTS**

Confocal microscope images of antibody penetration after 1, 2, 3, and 24 h incubation with J591-FITC are shown in Fig. 2. The images

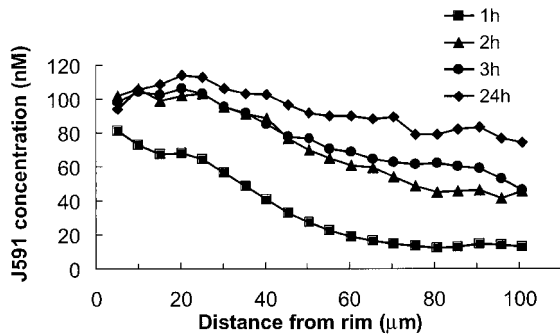


Fig. 3. Mean attenuation-corrected J591 concentration profiles in LNCaP-LN3 spheroids after 1-, 2-, 3-, and 24-h incubation with the antibody. Profiles were obtained by imaging five spheroids/time point.

show tightly packed cells filling the spheroid volumes, with the FITC label as the darker areas. The antibody is capable of reaching the core after approximately four half-lives of <sup>213</sup>Bi. No binding was observed in spheroids incubated with the FITC-labeled control antibody, HuM195-FITC (not shown). The attenuation-corrected antibody concentration profiles for four different incubation periods are shown in Fig. 3 as a function of distance from the rim of the spheroids.

Growth curves for individual spheroids of initial diameter 130 μm are shown in Fig. 4 after 24 h incubation with 0.9 and 1.8 MBq/ml <sup>213</sup>Bi-J591. Response after treatment with <sup>213</sup>Bi-HuM195 is shown as control. The growth curve in Fig. 4d was stopped at day 29 because of contamination of the culture plate. Spheroids irradiated with acute doses of 9 (Fig. 4a) and 12 Gy (Fig. 4b) external beam are shown in Fig. 5. Median spheroid volumes for spheroids incubated with 0.9 MBq/ml <sup>213</sup>Bi are compared with response after 9 and 12 Gy external beam photon irradiation in Fig. 6. The regrowth curves for all groups of treated spheroids were significantly different (*P* < 0.001) from the control spheroids, except for the group treated with unlabeled J591. No significant difference was found between spheroids incubated 24 h

Fig. 4. Individual growth curves for spheroids with initial diameters of 130 ± 20 μm after a 24-h incubation with 0.9 MBq/ml <sup>213</sup>Bi-J591 (a), 1.8 MBq/ml <sup>213</sup>Bi-J591 (b), 0.9 MBq/ml <sup>213</sup>Bi-HuM195 (nonspecific antibody; c), and 1.8 MBq/ml <sup>213</sup>Bi-HuM195 (nonspecific antibody; d).

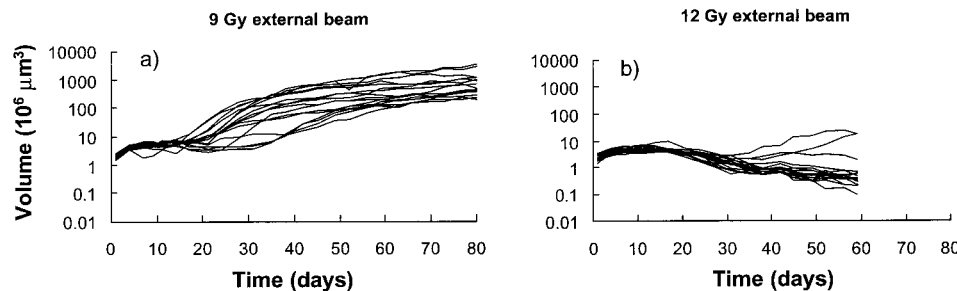
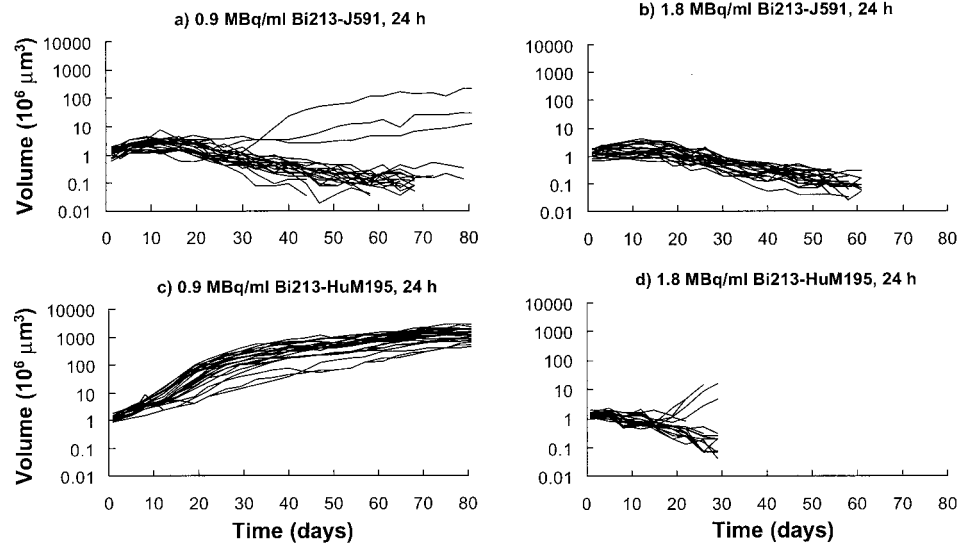


Fig. 5. Growth curves of individual spheroids after irradiation with an acute dose of 9 (a) and 12 (b) Gy external beam irradiation.

with 0.9 MBq/ml <sup>213</sup>Bi-J591 and those irradiated with 12 Gy external beam irradiation or between the spheroids incubated with <sup>213</sup>Bi-J591 for 60 min and those irradiated with 9 Gy external beam. The estimated mean absorbed dose to spheroids treated with 0.9 MBq/ml <sup>213</sup>Bi-J591 for 24 h was 3.7 Gy, suggesting a relative biological effectiveness factor of 3 over photon irradiation in this system.

To evaluate the impact of initial diameter on treatment response, growth curves for spheroids of initial median diameter of 180 μm were exposed to the same activity concentrations and incubation times as for the 130-μm-diameter spheroids. Growth curves for 180-μm-diameter spheroids are shown in Fig. 7. Monte Carlo-derived spatial dose distributions for 130- and 180-μm-diameter spheroids after treatment with 0.9 and 1.8 MBq/ml <sup>213</sup>Bi-J591 and HuM195 are shown in Fig. 8. Mean absorbed dose and spheroid fragmentation are summarized in Tables 1 and 2.

Light microscope images of one spheroid fragmenting (Fig. 9a), and one spheroid regrowing after 24 h incubation with 0.9 MBq/ml <sup>213</sup>Bi-J591 (Fig. 9b), and a <sup>213</sup>Bi-HuM195 treated spheroid (Fig. 9c) are shown. Four days after treatment, a 30–40-μm shell of shedding cells is observed in the spheroids treated with the specific antibody.

### DISCUSSION

Progression of prostate cancer is characterized by the dissemination of malignant prostatic epithelial cells and small clusters in the marrow. In advanced disease, such clusters remain small in size but

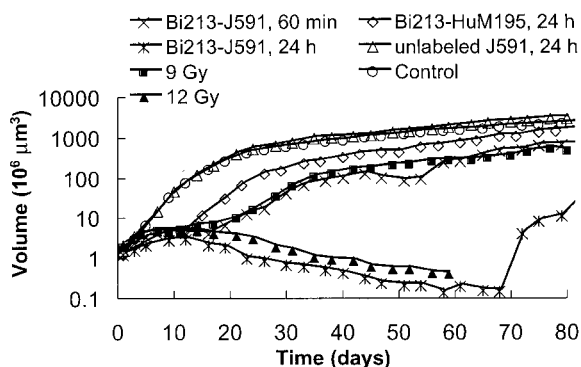


Fig. 6. Median spheroid volumes for spheroids incubated with 0.9 MBq/ml <sup>213</sup>Bi compared with response after 9 and 12 Gy external beam photon irradiation.

Fig. 7. Individual growth curves for spheroids with initial diameters 180 ± 20 μm after a 24-h incubation with 0.9 MBq/ml <sup>213</sup>Bi-J591 (a), 1.8 MBq/ml <sup>213</sup>Bi-J591 (b), 0.9 MBq/ml <sup>213</sup>Bi-HuM195 (nonspecific antibody; c), and 1.8 MBq/ml <sup>213</sup>Bi-HuM195 (nonspecific antibody; d).

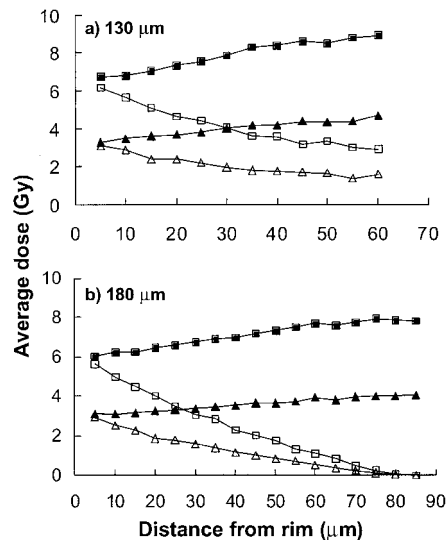
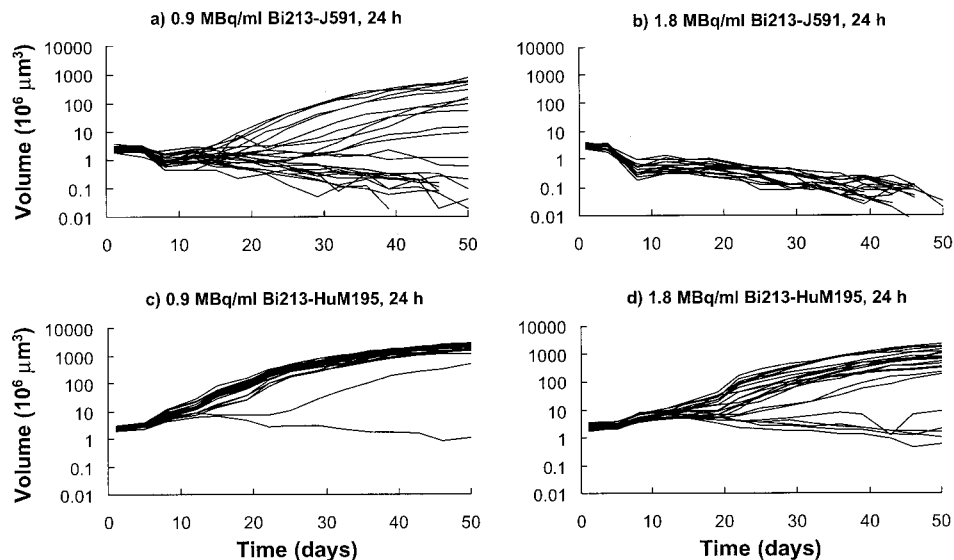


Fig. 8. Absorbed dose distribution for 130- and 180-μm spheroids treated with 0.9 MBq/ml <sup>213</sup>Bi-J591 (▲) and HuM195 (△), and 1.8 MBq/ml <sup>213</sup>Bi-J591 (■) and HuM195 (□).

Table 1 Average absorbed dose estimates to spheroids

Treatment group	Absorbed dose (Gy)			
	130-μm-diameter spheroid		180-μm-diameter spheroid	
	Specific	Nonspecific	Specific	Nonspecific
0.9 MBq/ml <sup>213</sup> Bi, 24 h	3.7	2.5	3.3	1.9
1.8 MBq/ml <sup>213</sup> Bi, 24 h	7.3	5.0	6.6	3.7

increase in frequency throughout the marrow and skeleton (28). The extravascular space of bone marrow is rapidly accessible by i.v.-administered antibodies (39, 50, 51). Therefore, use of the spheroid model to examine α-emitter radioimmunotherapy of such metastases is particularly appropriate. This analysis suggests that treatment efficacy will critically depend upon the time at which therapy is implemented relative to the time course of metastatic dissemination. A treatment strategy in which the α-emitter-labeled antibody is used to target disseminated micrometastatic deposits in the vasculature or bone marrow of prostate cancer patients when a prostate-specific

Table 2 Spheroid fragmentation (24 spheroids initially in each group)

Treatment group	No. of intact spheroids remaining			
	130-μm-diameter spheroid		180-μm-diameter spheroid	
	Specific	Nonspecific	Specific	Nonspecific
0.9 MBq/ml <sup>213</sup> Bi, 24 h	3	24	10	23
1.8 MBq/ml <sup>213</sup> Bi, 24 h	0	n/a	0	19

antigen recurrence is first observed may reduce metastatic spread. Alternatively, a multi-injection treatment approach in which the interval between treatment is chosen so as to shift, with each successive treatment, the size distribution of micrometastases toward smaller diameter clusters is also likely to be effective. Longer-lived, α-particle-emitting radionuclides such as <sup>211</sup>At (half-life, 7.2 h; Ref. 52) and <sup>225</sup>Ac (half-life, 10 days; Ref. 53) may also provide an advantage if their toxicity is acceptable. Because of their longer half-life, these radionuclides are less susceptible to loss of activity because of the slow antibody penetration kinetics seen in micrometastases.

Extrapolation of the experimental conditions used in this study to a human administration assuming antibodies are initially confined to a vascular and extracellular fluid volume of 3.8 liters (plasma volume plus extracellular fluid of liver, spleen, and marrow; Ref. 54), corresponds to an i.v. injection of 3.4 GBq <sup>213</sup>Bi on 38 mg of antibody. In patients with leukemia, wherein localization of radiolabeled antibody occurred primarily in the marrow, 2.6 GBq of <sup>213</sup>Bi were administered with no evidence of dose-limiting toxicity. Furthermore, the hematological toxicity observed was not qualitatively different from that obtained in a similar population of patients treated with a β-emitter conjugated to the same antibody (55).

Fig. 2 shows that at an antibody concentration of 10 μg/ml, corresponding to 38 mg of antibody in a human antibody penetration is relatively slow, given the short half-life of <sup>213</sup>Bi. By 2 h, 76% of all <sup>213</sup>Bi decays have already occurred. As shown in Fig. 2, complete penetration of spheroids by antibody is not achieved prior to 3 h. The 81-μm range of the emitted α compensates for this, however, and as shown in the growth delay curves, a clinically achievable activity concentration yields substantial spheroid volume reduction. However, as demonstrated by the response of 180-μm-diameter spheroids (Fig. 7) relative to the 130-μm-diameter spheroids (Fig. 4), the size distribution of micrometastases will have a critical impact on the efficacy of the treatment approach outlined above.

In Fig. 4a, three spheroids appear to be nonresponsive. The volumes of these are still 10- to 100-fold lower in volume than the hot control growth curves shown in Fig. 4c. We have no definitive explanations for why these three spheroids did not undergo fragmentation. It is possible that they reflect a heterogeneity in antigen expression, possibly derived from a subpopulation of cells whose antigen density was lower than the typical expression density of the cell population overall. The results depicted in Fig. 4d reflect “overkill,” *i.e.*, the activity concentration used is higher than the threshold value for avoiding “toxicity” (characterized by substantial fragmentation of spheroids treated by radiolabeled, nonspecific antibody). Although the response shown in Fig. 4b is excellent, it comes at the price of greater toxicity. This result is consistent with the dose calculations depicted in Fig. 8a, showing that the absorbed dose profile from the nonspecific antibody at the high concentration is greater for a significant portion of the spheroid volume than the dose delivered by the specific antibody at the lower activity concentration. The results suggest that for 130-μm-diameter tumor cell clusters, the optimal activity concentration for achieving a response lies between 0.9 and 1.8 MBq/ml <sup>213</sup>Bi.

In Fig. 6, the rise seen in the Bi-213-J591, 24-h curve after day 70 may be explained by examining Fig. 4. The rise beyond day 70 reflects the disaggregation of spheroids represented by most of the declining growth curves so that the median value beyond 70 days is after the rising growth curves. The rise in the median is sharper than any of the individual spheroid curves because the first post-70 day point is the average of the third and fourth curves (from the top), whereas the second and third point is obtained from the third curve. There is a fourth point, not shown on the plot at *d* = 82 that explains the apparent rise seen beyond day 79. This point is obtained from the second curve because spheroids corresponding to the two lower curves have disaggregated by day 82.

As shown in Fig. 8, the spatial distribution of absorbed dose throughout both 130- and 180-μm-diameter spheroids, treated with the specific antibody, is generally uniform with a 1.3–1.4-fold “cross-fire”-related increase in the absorbed dose near the center of the spheroids. The reduction in efficacy seen between the two spheroid sizes does not, therefore, arise because a portion of the larger spheroid volume remains unirradiated but rather is attributable to the increase in cell number that must be sterilized to achieve spheroid fragmentation. Approximately 600 cells make up 130-μm-diameter spheroids; the number doubles to 1200 cells for 180-μm-diameter spheroids. By convolving an α-particle radiosensitivity derived from LNCaP cells grown in monolayer with the mean absorbed dose in each 5-μm-thick shell, it is possible to estimate that ~4 of 600 cells may be expected

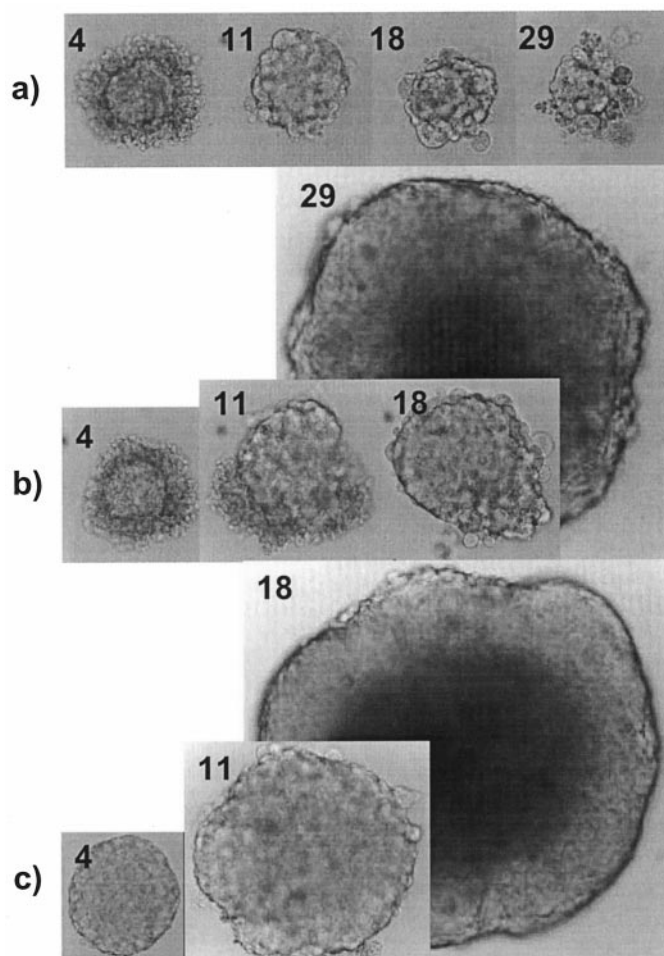


Fig. 9. Light microscope images on days 4, 11, 18, and 29 of two spheroids treated with 0.9 MBq/ml <sup>213</sup>Bi-J591, where one spheroid fragmented (a) and one spheroid experienced a growth delay but then finally continued to grow (b). c, a hot control is shown on days 4, 11, and 18.

to survive in smaller spheroids treated with 0.9 MBq/ml. The corresponding number of cells for the larger spheroids is 12 of 1200. The difference in absolute number of cells remaining is likely to be responsible for the observed differences in treatment efficacy. In 180-μm-diameter spheroids treated with the higher, 1.8 MBq/ml exposure, the number of cells expected to survive is 0.17. The much lower cell survival expected in this case is consistent with the results shown on Table 2, wherein all 24 of the larger spheroids fragmented after a 1.8 MBq/ml exposure. It is important to recognize that the radiosensitivity of cells in spheroid culture *versus* monolayer culture differs for low linear energy transfer emissions (56) and may also differ for α-particles (19). Nevertheless, the analysis demonstrates that the difference in response between the 130- *versus* the 180-μm-diameter spheroids is not a result of diminished absorbed dose but rather may be explained on basic radiobiological grounds (57).

The radial absorbed dose distributions for spheroids treated with the nonspecific antibody suggest that the differences in fragmentation arise, in this case, in part because the 81-μm range of Bi-213 α-particle emissions is insufficient to reach the center of the larger spheroids. Correspondingly, no dose is delivered to the center of 180-μm-diameter spheroids treated with either 0.9 or 1.8 MBq/ml nonspecific antibody.

Comparing the median volume reduction curves of nonspecific and specific antibody (Fig. 6), a 10–15-day delay may be anticipated before a differential therapeutic effect is seen. The images in Fig. 9, however, suggest that this is a result of cell swelling prior to lysis and elimination (see Fig. 9a, day 4 *versus* day 11).

Bone involvement in prostate cancer is the most common and potentially the most debilitating site of spread (28). Disruption of the process by which tumor cells seed the marrow to form skeletal metastases would be of great therapeutic value. The studies and analyses described in this work support the use of α-emitter radioimmunotherapy with <sup>213</sup>Bi and an anti-PSMA antibody in such a treatment strategy. Animal studies (21) and results from a clinical trial in patients with leukemia (55) suggest that the toxicity of such an approach will not be prohibitive.

**ACKNOWLEDGMENTS**

Confocal microscopy imaging was performed in collaboration with Dr. Katia Manova, director of the Molecular Cytology Core Facility, Memorial Sloan-Kettering Cancer Center. Cells expressing green fluorescent protein were kindly provided by Drs. Steven Larson and Bipin Mehta of the Nuclear Medicine Research Laboratory, Sloan-Kettering Institute. <sup>225</sup>Ac for <sup>213</sup>Bi generation was provided by PharmActinium, Inc., Chevy Chase, MD; The Institute for Transuranic Elements, Karlsruhe, Germany; and the Department of Energy, Isotopes Production, and Distribution.

**REFERENCES**

1. Kaminski, M. S., Zasadny, K. R., Francis, I. R., Milik, A. W., Ross, C. W., Moon, S. D., Crawford, S. M., Burgess, J. M., Petry, N. A., Butchko, G. M., *et al.* Radioimmunotherapy of B-cell lymphoma with [<sup>131</sup>I]anti-B1 (anti-CD20) antibody. *N. Engl. J. Med.*, *329*: 459–465, 1993.
2. Press, O. W., Eary, J. F., Appelbaum, F. R., Martin, P. J., Badger, C. C., Nelp, W. B., Glenn, S., Butchko, G., Fisher, D., Porter, B., *et al.* Radiolabeled-antibody therapy of B-cell lymphoma with autologous bone marrow support. *N. Engl. J. Med.*, *329*: 1219–1224, 1993.
3. Witzig, T. E., White, C. A., Wiseman, G. A., Gordon, L. I., Emmanouilides, C., Raubitschek, A., Janakiramam, N., Gutheil, J., Schilder, R. J., Spies, S., Silverman, D. H., Parker, E., and Grillo-Lopez, A. J. Phase I/II trial of IDEC-Y2B8 radioimmunotherapy for treatment of relapsed or refractory CD20(+) B-cell non-Hodgkin's lymphoma. *J. Clin. Oncol.*, *17*: 3793–3803, 1999.
4. Gerlowski, L. E., and Jain, R. K. Microvascular permeability of normal and neoplastic tissues. *Microvasc. Res.*, *31*: 288–305, 1986.
5. Dvorak, H. F., Nagy, J. A., Dvorak, J. T., and Dvorak, A. M. Identification and characterization of the blood vessels of solid tumors that are leaky to circulating macromolecules. *Am. J. Pathol.*, *133*: 95–109, 1988.

6. Jain, R. K., and Baxter, L. T. Mechanisms of heterogeneous distribution of monoclonal antibodies and other macromolecules in tumors: significance of elevated interstitial pressure. *Cancer Res.*, *48*: 7022–7032, 1988.
7. Clauss, M. A., and Jain, R. K. Interstitial transport of rabbit and sheep antibodies in normal and neoplastic tissues. *Cancer Res.*, *50*: 3487–3492, 1990.
8. Fujimori, K., Covell, D. G., Fletcher, J. E., and Weinstein, J. N. A modeling analysis of monoclonal antibody percolation through tumors: a binding-site barrier. *J. Nucl. Med.*, *31*: 1191–1198, 1990.
9. Sgouros, G. Plasmapheresis in radioimmunotherapy of micrometastases: a mathematical modeling and dosimetrical analysis. *J. Nucl. Med.*, *33*: 2167–2179, 1992.
10. Macklis, R. M., Kinsey, B. M., Kassis, A. I., Ferrara, J. L., Atcher, R. W., Hines, J. J., Coleman, C. N., Adelstein, S. J., and Burakoff, S. J. Radioimmunotherapy with α-particle-emitting immunoconjugates. *Science (Washington DC)*, *240*: 1024–1026, 1988.
11. Humm, J. L., and Chin, L. M. A model of cell inactivation by α-particle internal emitters. *Radiat. Res.*, *134*: 143–150, 1993.
12. Sutherland, R. M. Cell and environment interactions in tumor microregions: the multicell spheroid model. *Science (Washington DC)*, *240*: 177–184, 1988.
13. Walker, K. A., Murray, T., Hilditch, T. E., Wheldon, T. E., Gregor, A., and Hann, I. M. A tumor spheroid model for antibody-targeted therapy of micrometastases. *Br. J. Cancer*, *58*: 13–16, 1988.
14. Kwok, C. S., Crivici, A., MacGregor, W. D., and Unger, M. W. Optimization of radioimmunotherapy using human malignant melanoma multicell spheroids as a model. *Cancer Res.*, *49*: 3276–3281, 1989.
15. Bardies, M., Thedrez, P., Gestin, J. F., Marcille, B. M., Guereau, D., Faivre-Chauvet, A., Mahe, M., Sai-Maurel, C., and Chatal, J. F. Use of multi-cell spheroids of ovarian carcinoma as an intraperitoneal radio-immunotherapy model: uptake, retention kinetics, and dosimetric evaluation. *Int. J. Cancer*, *50*: 984–991, 1992.
16. Essand, M., Nilsson, S., and Carlsson, J. Growth of prostatic cancer cells, DU 145, as multicellular spheroids and effects of estramustine. *Anticancer Res.*, *13*: 1261–1268, 1993.
17. Ballangrud, A. M., Yang, W. H., Dnistrian, A., Lampen, N. M., and Sgouros, G. Growth and characterization of LNCaP prostate cancer cell spheroids. *Clin. Cancer Res.*, *5*: 3171s–3176s, 1999.
18. Langmuir, V. K., McGann, J. K., Buchegger, F., and Sutherland, R. M. <sup>131</sup>I-anticarcinoembryonic antigen therapy of LS174T human colon adenocarcinoma spheroids. *Cancer Res.*, *49*: 3401–3406, 1989.
19. Kennel, S. J., Stabin, M., Roeske, J. C., Foote, L. J., Lankford, P. K., Terzaghi-Howe, M., Patterson, H., Barkenbus, J., Popp, D. M., Boll, R., and Mirzadeh, S. Radiotoxicity of bismuth-213 bound to membranes of monolayer and spheroid cultures of tumor cells. *Radiat. Res.*, *151*: 244–256, 1999.
20. Behr, T. M., Behe, M., Stabin, M. G., Wehrmann, E., Apostolidis, C., Molinet, R., Strutz, F., Fayyazi, A., Wieland, E., Gratz, S., Koch, L., Goldenberg, D. M., and Becker, W. High-linear energy transfer (LET) α *versus* low-LET β emitters in radioimmunotherapy of solid tumors: therapeutic efficacy and dose-limiting toxicity of <sup>213</sup>Bi- *versus* <sup>90</sup>Y-labeled CO17-1A Fab' fragments in a human colonic cancer model. *Cancer Res.*, *59*: 2635–2643, 1999.
21. Behr, T. M., Sgouros, G., Stabin, M. G., Behe, M., Angerstein, C., Blumenthal, R. D., Apostolidis, C., Molinet, R., Sharkey, R. M., Koch, L., Goldenberg, D. M., and Becker, W. Studies on the red marrow dosimetry in radioimmunotherapy: an experimental investigation of factors influencing the radiation-induced myelotoxicity in therapy with β-, Auger/conversion electron-, or α-emitters. *Clin. Cancer Res.*, *5*: 3031s–3043s, 1999.
22. Kennel, S. J., and Mirzadeh, S. Vascular targeted radioimmunotherapy with <sup>213</sup>Bi- an α-particle emitter. *Nucl. Med. Biol.*, *25*: 241–246, 1998.
23. Zalutsky, M. R., McLendon, R. E., Garg, P. K., Archer, G. E., Schuster, J. M., and Bigner, D. D. Radioimmunotherapy of neoplastic meningitis in rats using an α-particle-emitting immunoconjugate. *Cancer Res.*, *54*: 4719–4725, 1994.
24. Jurcic, J. G., McDevitt, M. R., Sgouros, G., Ballangrud, A. M., Finn, R. D., Geerlings, M. W., Humm, J. L., Molinet, R., Apostolidis, C., Larson, S. M., and Scheinberg, D. A. Targeted α-particle therapy for myeloid leukemias: a Phase I trial of bismuth-213-HuM195 (anti-CD33). *Blood*, *90*: 2245, 1997.
25. Sgouros, G., Ballangrud, A. M., Jurcic, J. G., McDevitt, M. R., Humm, J. L., Erdi, Y. E., Mehta, B. M., Finn, R. D., Larson, S. M., and Scheinberg, D. A. Pharmacokinetics and dosimetry of an α-particle emitter labeled antibody: <sup>213</sup>Bi-HuM195 (anti-CD33) in patients with leukemia. *J. Nucl. Med.*, *40*: 1935–1946, 1999.
26. Zalutsky, M. R., and Vaidyanathan, G. Astatine-211-labeled radiotherapeutics: an emerging approach to targeted α-particle radiotherapy. *Curr. Pharm. Des.*, *6*: 1433–1455, 2000.
27. Zalutsky, M. R., Cokgor, I., Akabani, G., Friedman, H. S., Coleman, R. E., Friedman, A. H., McLendon, R. E., Reist, C. J., Pegram, C. M., Zhao, X. G., and Bigner, D. D. Phase I trial of α-particle-emitting astatine-211 labeled chimeric antitenascin antibody in recurrent malignant glioma patients. *Proc. Am. Assoc. Cancer Res.*, *41*: 544, 2000.
28. Scher, H. I., and Cheung, L. W. K. Bone metastases: biology and therapy. *Semin. Oncol.*, *21*: 630–656, 1994.
29. Haq, M., Goltzman, D., Tremblay, G., and Brodt, P. Rat prostate adenocarcinoma cells disseminate to bone and adhere preferentially to bone marrow-derived endothelial cells. *Cancer Res.*, *52*: 4613–4619, 1992.
30. Pettaway, C. A., Pathak, S., Greene, G., Ramirez, E., Wilson, M. R., Killion, J. J., and Fidler, I. J. Selection of highly metastatic variants of different human prostatic carcinomas using orthotopic implantation in nude mice. *Clin. Cancer Res.*, *2*: 1627–1636, 1996.
31. Horoszewicz, J. S., Leong, S. S., Kawinski, E., Karr, J. P., Rosenthal, H., Chu, T. M., Mirand, E. A., and Murphy, G. P. LNCaP model of human prostatic carcinoma. *Cancer Res.*, *43*: 1809–1818, 1983.

32. Israeli, R. S., Powell, C. T., Corr, J. G., Fair, W. R., and Heston, W. D. Expression of the prostate-specific membrane antigen. *Cancer Res.*, *54*: 1807–1811, 1994.
33. Yuhas, J. M., Li, A. P., Martinez, A. O., and Ladman, A. J. A simplified method for production and growth of multicellular tumor spheroids. *Cancer Res.*, *37*: 3639–3643, 1977.
34. Liu, H., Moy, P., Kim, S., Xia, Y., Rajasekaran, A., Navarro, V., Knudsen, B., and Bander, N. H. Monoclonal antibodies to the extracellular domain of prostate-specific membrane antigen also react with tumor vascular endothelium. *Cancer Res.*, *57*: 3629–3634, 1997.
35. Liu, H., Rajasekaran, A. K., Moy, P., Xia, Y., Kim, S., Navarro, V., Rahmati, R., and Bander, N. H. Constitutive and antibody-induced internalization of prostate-specific membrane antigen. *Cancer Res.*, *58*: 4055–4060, 1998.
36. McDevitt, M. R., Barendsward, E., Ma, D., Lai, L., Curcio, M. J., Sgouros, G., Ballangrud, A. M., Yang, W. H., Finn, R. D., Pelligreni, V., Geerlings, M. W., Jr., Brechbiel, M. W., Bander, N. H., and Scheinberg, D. A. An  $\alpha$ -particle emitting bismuth-213 labeled antibody (J591) to the external domain of prostate specific membrane antigen. *Cancer Res.*, *60*: 6095–6100, 2000.
37. Mason, D. W., and Williams, A. F. The kinetics of antibody binding to membrane antigens in solution and at the cell surface. *Biochem. J.*, *187*: 1–20, 1980.
38. Silver, D. A., Pellicer, I., Fair, W. R., Heston, W. D., and Cordon-Cardo, C. Prostate-specific membrane antigen expression in normal and malignant human tissues. *Clin. Cancer Res.*, *3*: 81–85, 1997.
39. Scheinberg, D. A., Tanimoto, M., McKenzie, S., Strife, A., Old, L. J., and Clarkson, B. D. Monoclonal antibody M195: a diagnostic marker for acute myelogenous leukemia. *Leukemia (Baltimore)*, *3*: 440–445, 1989.
40. Tanimoto, M., Scheinberg, D. A., Cordon-Cardo, C., Huie, D., Clarkson, B. D., and Old, L. J. Restricted expression of an early myeloid and monocytic cell surface antigen defined by monoclonal antibody M195. *Leukemia (Baltimore)*, *3*: 339–348, 1989.
41. Brechbiel, M. W., Pippin, C. G., McMury, T. J., Milenic, D., Roselli, M., Colcher, D., and Gansow, O. A. An effective chelating agent for labeling of monoclonal antibody with  $^{212}\text{Bi}$  for  $\alpha$ -particle mediated radioimmunotherapy. *J. Chem. Soc. Chem. Commun.*, *17*: 1169–1170, 1991.
42. Brechbiel, M. W., and Gansow, O. A. Synthesis of C-functionalized *trans*-cyclohexyldiethylenetriaminepenta-acetic acids for labeling of monoclonal antibodies with bismuth-212  $\alpha$ -particle emitter. *J. Chem. Soc. Perkin Trans. I*, *1*: 1173–1178, 1992.
43. Nikula, T. K., McDevitt, M. R., Finn, R. D., Wu, C., Kozak, R. W., Garmestani, K., Brechbiel, M. W., Curcio, M. J., Pippin, C. G., Tiffany-Jones, L., Geerlings, M. W., Sr., Apostolidis, C., Molinet, R., Geerlings, M. W., Jr., Gansow, O. A., and Scheinberg, D. A.  $\alpha$ -Emitting bismuth cyclohexylbenzyl DTPA constructs of recombinant humanized anti-CD33 antibodies: pharmacokinetics, bioactivity, toxicity, and chemistry. *J. Nucl. Med.*, *40*: 166–176, 1999.
44. McDevitt, M. R., Finn, R. D., Ma, D., Larson, S. M., and Scheinberg, D. A. Preparation of  $\alpha$ -emitting  $^{213}\text{Bi}$ -labeled antibody constructs for clinical use. *J. Nucl. Med.*, *40*: 1722–1727, 1999.
45. McDevitt, M. R., Finn, R. D., Sgouros, G., Ma, D., and Scheinberg, D. A. An  $^{225}\text{Ac}/^{213}\text{Bi}$  generator system for therapeutic clinical applications: construction and operation. *Appl. Radiat. Isot.*, *50*: 895–904, 1999.
46. Kolbert, K. S., Hamacher, K. A., Jurcic, J. G., Scheinberg, D. A., Larson, S. M., and Sgouros, G. Parametric images of antibody pharmacokinetics in  $^{213}\text{Bi}$ -HuM195 therapy of leukemia. *J. Nucl. Med.*, *42*: 27–32, 2001.
47. Charlton, D. E. Radiation effects in spheroids of cells exposed to  $\alpha$  emitters. *Int. J. Radiat. Biol.*, *76*: 1555–1564, 2000.
48. Ziegler, J. Stopping and range of ions in matter (SRIM96). *In*: IBM Research. Yorktown, NY: IBM Corp., 1996.
49. Zeger, S. L., and Liang, K. Y. Longitudinal data analysis for discrete and continuous outcomes. *Biometrics*, *42*: 121–130, 1986.
50. Sgouros, G., Graham, M. C., Divgi, C. R., Larson, S. M., and Scheinberg, D. A. Modeling and dosimetry of monoclonal antibody M195 (anti-CD33) in acute myelogenous leukemia. *J. Nucl. Med.*, *34*: 422–430, 1993.
51. Sgouros, G. Bone marrow dosimetry for radioimmunotherapy: theoretical considerations. *J. Nucl. Med.*, *34*: 689–694, 1993.
52. Zalutsky, M. R., and Bigner, D. D. Radioimmunotherapy with  $\alpha$ -particle-emitting radioimmunoconjugates. *Acta Oncol.*, *35*: 373–379, 1996.
53. McDevitt, M. R., Sgouros, G., Finn, R. D., Humm, J. L., Jurcic, J. G., Larson, S. M., and Scheinberg, D. A. Radioimmunotherapy with  $\alpha$ -emitting nuclides. *Eur. J. Nucl. Med.*, *25*: 1341–1351, 1998.
54. Snyder, W. S., Cook, M. J., Nasset, E. S., Karhausen, L. R., Howells, G. P., and Tipton, I. H. Report of the task group on reference man. *In*: ICRP Publication, Vol. 23. Elmsford, NY: International Commission on Radiological Protection, 1975.
55. Sgouros, G., Ballangrud, A. M., Jurcic, J. G., Panageas, K. S., McDevitt, M. R., Finn, R. D., Larson, S. M., and Scheinberg, D. A.  $\beta$  versus  $\alpha$ -emitter dose-response analysis in patients. *J. Nucl. Med.*, *41*: 82P, 2000.
56. Olive, P. L., and Durand, R. E. Drug and radiation resistance in spheroids: cell contact and kinetics. *Cancer Metastasis Rev.*, *13*: 121–138, 1994.
57. O'Donoghue, J. A., Bardies, M., and Wheldon, T. E. Relationships between tumor size and curability for uniformly targeted therapy with  $\beta$ -emitting radionuclides. *J. Nucl. Med.*, *36*: 1902–1909, 1995.